Ion charge state distributions of vacuum arc plasmas: The origin of species

André Anders
Ernest O. Lawrence Berkeley National Laboratory, University of California, Berkeley, California 94720
(Received 6 May 1996)

Vacuum arc plasmas are produced at micrometer-size, nonstationary cathode spots. Ion charge state distributions (CSD's) are experimentally known for 50 elements, but the theoretical understanding is unsatisfactory. In this paper, CSD's of vacuum arc plasmas are calculated under the assumption that the spot plasma experiences an instantaneous transition from equilibrium to nonequilibrium while expanding. Observable charge state distributions are the result of a freezing process at this transition. ''Frozen'' CSD's have been calculated using Saha equations in the Debye-Hückel approximation of the nonideal plasma for all metals of the Periodic Table and for boron, carbon, silicon, and germanium. The results are presented in a ''periodic table of CSD.'' The table contains also the mean ion charge state, the neutral vapor fraction, and the effective plasma temperature and density at the freezing point for each element. The validity of the concepts of ''instantaneous freezing'' and ''effective temperature and density'' is discussed for low and high currents and for the presence of a magnetic field. Temperature fluctuations have been identified to cause broadening of CSD's.
[S1063-651X(97)07201-2]

PACS number(s): 52.80.Vp

I. INTRODUCTION

The electrical current of an arc discharge between solid electrodes in vacuum is transported by the plasma produced by the discharge itself. The plasma usually originates from cathode spots: locations of very small area with very high current density, plasma density, and temperature [1–4]. The discharge is a low-current vacuum arc if the current is of order 100 A and the cathode-anode burning voltage about 20–25 V. The arc extinguishes if the current drops below the ''chopping current,'' which is typically a few amperes and depends on the cathode material [5,6]; the plasma production is obviously not sufficient to sustain the arc. The anode is passive at low currents and serves mainly as an electron collector. This changes at high currents: plasma is also produced at anode spots [7]. Another form of vacuum arc is observed when the anode is thermally isolated so that the discharge burns in the ionized vapor of anode material (''anodic'' vacuum arc [8–10]). A similar effect has been found for cathodes of low melting point and high vapor pressure (''spotless'' vacuum arcs [11,12]).

The observable charge state distribution (CSD) of ions is an important plasma feature that gives insight into the physics of plasma formation. Furthermore, high charge states are of practical interest for vacuum arc ion sources since the ion beam energy is proportional to the ion charge $E = QU_{\mathrm{extr}}$, where U_{extr} is the extractor voltage.

There is little information in the literature for the charge states of anodic vacuum arcs and spotless vacuum arcs. Generally it is assumed that heavy particles are either neutral atoms (metal vapor) or singly charged ions.

In contrast, CSDs of ions of low-current plasmas have been extensively studied using time-of-flight charge-to-mass spectrometry [13–22], motivated by the development of vacuum arc ion sources (see review [21]). These sources operate usually in a repetitively pulsed mode (arc duration of order 1 ms or less) with repetition rates of a few pulses per second, an arc current of 100–300 A, an ion beam current of order 100 mA (during pulses), and an extractor voltage in the range 20–100 kV. It has been found that there exist material-specific CSDs that depend very little on the current (current range 50–300 A [20]). Charge states are higher at the beginning of an arc discharge and become constant after about 100 μs [18,23]. The most complete table of CSDs (at arc current 100 A, measured about 100 μs after arc ignition) is given in Ref. [21] for 50 cathode materials; see also Table I. It has been found that the ion charge states can be enhanced by external magnetic fields [18–20,24] and by high discharge currents [22,25]. This effect is in agreement with spectroscopic investigations of short-pulse, high-current vacuum sparks [26,27], which show that ions of very high charge states exist for short times in small, magnetically compressed, nonstationary, hot plasmas.

In this paper we discuss the formation of ions in vacuum arc discharges (both low and high current) for all metallic elements of the Periodic Table based on the ideas that (i) local thermodynamic equilibrium (LTE) can be assumed in the vicinity of cathode spots [28], (ii) Saha equations of weakly nonideal plasmas (Debye-Hückel approximation) describe the CSDs correctly as long as LTE is valid, (iii) CSDs remain constant (they ''freeze'') when the plasmas expand into the vacuum and become non-LTE plasmas, and (iv) the fluctuations of plasma temperature and density at freezing are small enough to allow the introduction of an ''effective freezing temperature'' and an ''effective freezing density'' for each element.

II. PHASE TRANSITIONS

Ions in vacuum discharge plasmas originate from the metal electrodes (the formation of ions from oxide and water layers and other contaminates and insulators is usually small). In the case of ''spotless cathodic arcs'' and ''anodic arcs,'' melting and evaporation of the metal are ''conventional'' phase transitions that are observed at the cathode and anode, respectively. Large parts of the electrodes are suffi-

TABLE I. Elementary cathode materials, their nuclear charge number Z, melting point [54] (°C) boiling point [54] (°C), mean ion charge state [21] Q, and detailed distribution [21] (%, particle fraction). Note that the latter data are experimentally obtained by averaging over many individual discharges with arc currents of about 100 A.

Z	Element	T_{melt} (°C)	T_{boil} (°C)	$\overline{Q}$	f_1 (%)	f_2 (%)	f_3 (%)	f_4 (%)	f_5 (%)	f_6 (%)
3	Li	180.5	1347	1.00	100					
6	C	3550	4827	1.00	100					
12	Mg	648.8	1090	1.54	46	54				
13	Al	660.4	2467	1.73	38	51	11			
14	Si	1410	2355	1.39	63	35	2			
20	Ca	839	1484	1.93	8	91	1			
21	Sc	1541	2831	1.79	27	67	6			
22	Ti	1660	3287	2.03	11	75	14			
23	V	1890	3380	2.14	8	71	20	1		
24	Cr	1857	2672	2.09	10	68	21	1		
25	Mn	1244	1962	1.53	49	50	1			
26	Fe	1535	2750	1.82	25	68	7			
27	Co	1495	2870	1.73	34	59	7			
28	Ni	1453	2732	1.76	30	64	6			
29	Cu	1083	2567	2.06	16	63	20	1		
30	Zn	419.6	907.0	1.20	80	20				
32	Ge	937.4	2830	1.40	60	40				
38	Sr	769	1384	1.98	2	98				
39	Y	1522	3338	2.28	5	62	33			
40	Zr	1852	4377	2.58	1	47	45	7		
41	Nb	2468	4742	3.00	1	24	51	22	2	
42	Mo	2617	4612	3.06	2	21	49	25	3	
46	Pd	1552	3140	1.88	23	67	9	1		
47	Ag	1410	2355	2.14	13	61	25	1		
48	Cd	320.9	765	1.32	68	32				
49	In	156.6	2080	1.34	66	34				
50	Sn	232	2270	1.53	47	53				
51	Sb	630.7	1750	1.00	100					
56	Ba	725	1640	2.00	0	100				
57	La	921	3457	2.22	1	76	23			
58	Ce	799	3426	2.11	3	83	14			
59	Pr	931	3512	2.25	3	69	28			
60	Nd	1021	3068	2.17	0	83	17			
62	Sm	1077	1791	2.13	2	83	15			
64	Gd	1313	3266	2.20	2	76	22			
66	Dy	1412	2562	2.30	2	66	32			
67	Ho	1474	2695	2.30	2	66	32			
68	Er	1529	2863	2.36	1	63	35	1		
69	Tm	1545	1947	1.96	13	78	9			
70	Yb	819	1194	2.03	3	88	8			
72	Hf	2227	4602	2.89	3	24	51	21	1	
73	Ta	2996	5425	2.93	2	33	38	24	3	
74	W	3410	5660	3.07	2	23	43	26	5	1
77	Ir	2410	4130	2.66	5	37	46	11	1	
78	Pt	1772	3827	2.08	12	69	18	1		
79	Au	1064	2807	2.97	14	75	11			
82	Pb	327	1740	1.64	36	64				
83	Bi	271.3	1560	1.17	83	17				
90	Th	1750	4790	2.88	0	24	64	12		
92	U	1132	3818	3.18	0	12	58	30		

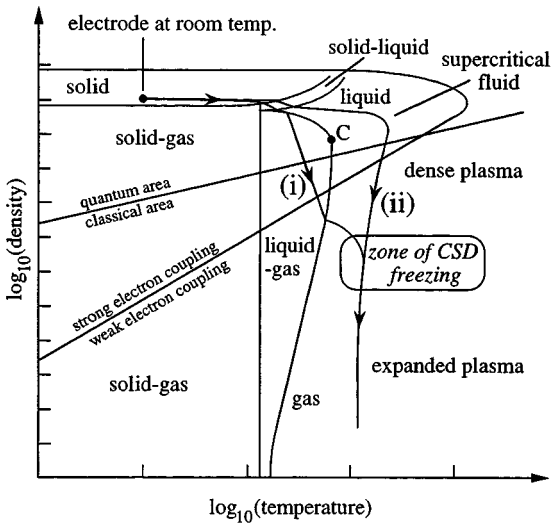

FIG. 1. Two limiting paths of electrode material in the density-temperature phase diagram: (i) ''conventional'' model, with melting, evaporation, and ionization and (ii) model of microexplosions, circumnavigating the critical point *C* (compare Ref. [33]). Note that both paths merge approximately in the zone where the CSD freezes.

ciently hot to produce metal vapor that becomes partially ionized by the electron current. The electron temperature was found to be low (0.4–0.9 eV for a 25-A aluminum anodic arc) and, not surprisingly, about only 10% of the evaporated atoms were ionized with single charge state [9]. A similar situation can be assumed for spotless cathodic arcs.

The situation is different when the electrodes remain globally cold so that evaporation is negligible. The discharge current is concentrated at spots at the cathode if the current is low (say, less than 1 kA) or at both the cathode and anode if the current is high. Spot formation happens to ensure sufficient electron emission and plasma production necessary to transport the charge between electrodes. In this paper we focus on the formation of ions in the vicinity of cathode spots.

The case of cathode spots of low-current vacuum arc discharges without external magnetic field has been discussed in a number of papers [29–37]. Although it is clear that the electrode material is transformed from solid metal into low-density, expanding plasma, it is not obvious which path the material takes in the phase diagram. There are two limiting cases possible (Fig. 1): (i) atoms evaporate at the very high spot temperature and become ionized by electrons that are accelerated in the cathode voltage drop (this is a picture similar to conventional models of gaseous arcs) and (ii) the cathode material transforms from solid metal to liquid metal and then continuously to dense high-pressure, nonideal plasma followed by low-density, expanded, nonequilibrium plasma. Recent experiments [38–40] have confirmed that model (ii) is applicable to at least the formation periods of ''microspots'' or ''fragments'' of cathode spots. Theory and experiments indicate that probably both models are justified: model (ii) describes the initial and active phase of a microspot, while model (i) refers to the final phase of the microspot lifetime. The cathode material is heated by two main mechanisms: ion bombardment (from the plasma above the cathode surface) and Joule heating. The Nottingham effect can also contribute to heating (heating or cooling is possible [41,42]). Runaway Joule heating is important for vacuum breakdown and ion bombardment heating is dominant once the plasma is formed in front of the cathode [43].

Interestingly, both limiting paths start at the same point and merge at the zone where the freezing of ion charge states is expected. Therefore, the model calculation does not allow for conclusions regarding the path of the material in the phase diagram.

III. NONIDEAL PLASMAS AND SAHA EQUATIONS

The high local power density at the electrode surface leads to the formation of a small, dense plasma. This is true in both models previously described, but the plasma density in model (ii) is greater by orders of magnitude. Dense plasmas are characterized by a strong interaction between plasma particles and therefore they are often called ''strongly coupled'' or ''nonideal'' plasmas. There are several dimensionless parameters describing the degree a plasma being nonideal or strongly coupled; see definitions in Refs. [44–46]. Most laboratory plasmas are ideal, i.e., the potential energy of the Coulomb interaction between charged particles is much smaller than their average kinetic energy. At high densities, the Coulomb interaction of the outer bound electrons of atoms and ions with their surrounding charged particles (ions and free electrons) and polarizable particles (atoms and clusters) leads to a substantial shift of energy levels and the lowering of the binding energy of bound electrons [47]. As a result, a sharp increase in the ionization state of the plasma is observed at high density (pressure); this effect is sometimes called ''pressure ionization'' or ''pressure-induced ionization'' [33,48].

The ion charge state distribution of a plasma in equilibrium can be calculated using a set of Saha equations of the form

$$\frac{n_e n_{Q+1}}{n_Q} = \Lambda_B^{-3} \frac{2\Sigma_{Q+1}(T)}{\Sigma_Q(T)} \exp\left(-\frac{E_Q - \Delta E_Q}{kT}\right), \quad Q = 0,1,2,\ldots,Q_{\max}, \qquad (1)$$

where n_e and n_Q are the density of free electrons and ions of charge state Q, respectively, $Q=0$ for neutral atoms, $Q=1$ for singly ionized ions, etc., with $Q_{\max}$ the maximum charge state abundant in the plasma; $\Sigma_Q(T)$ is the temperature-dependent partition function of ions of charge state Q, k is the Boltzmann constant, T is the temperature,

$$\Lambda_B = h/(2\pi m_e kT)^{1/2} \qquad (2)$$

is the thermal de Broglie wavelength, and E_Q is the ionization energy of the Q-fold charged ion. The lowering of the ionization energy ΔE_Q reflects the particle interaction or nonideal nature of the plasma.

A rigorous expression for ΔE_Q can be found in [33], where electron degeneration have been taken into account and the Coulomb interaction is written as a Padé approximation to interpolate between the quantum-corrected Debye law and analytical expressions for the strongly coupled ionic subsystem that is screened by a ''liquid'' of degenerated electrons; short-range repulsion between shells of bound elec-

trons of different ions is taken into account by a hard-core interaction [49]. In this way, compositions of nonideal plasmas with densities of heavy particles as high as 10^{29} m^{-3} can be calculated.

For weakly or moderately nonideal plasmas (i.e., the degeneration of electrons is not considered and quantum-mechanical exchange interaction between bound-shell electrons of neighboring ions can be neglected), the lowering of the ionization energies can be described by the relatively simple Debye-Hückel theory [45]

$$\Delta E_Q = \frac{(Q+1)e^2}{4\pi\varepsilon_0(\lambda_D+\Lambda_B/8)}, \tag{3}$$

where

$$\lambda_D = \left\{ \varepsilon_0 kT \Big/ \left[e^2 \left(n_e + \sum_Q Q^2 n_Q \right) \right] \right\}^{1/2} \tag{4}$$

is the Debye length and ε_0 is the permittivity of vacuum.

The partition function reflects the structure of the electron shells and is defined by the equation [50]

$$\Sigma_Q(T) = \sum_{s=1}^{s=s_{\max}} g_{Q,s} \exp\left(-\frac{E_{Q,s}}{kT} \right), \tag{5}$$

where s is the level index ($s=1$ is the ground state, $s_{\max}$ is the highest excited level that is bound) and $g_{Q,s}$ and $E_{Q,s}$ are the statistical weight and the energy of level s of an ion with charge state Q, respectively. The statistical weight $g_{Q,s}=2J_{Q,s}+1$ can be obtained using the total angular momentum $J_{Q,s}$ given in spectral tables such as those in [51–53]. The system of equations (1)–(5) is completed by the charge-neutrality condition

$$n_e = \sum_Q^{Q_{\max}} Q n_Q . \tag{6}$$

The results of the calculations are presented using the following definitions. The percentages of ion charge states are expressed as particle fractions of all ions (not heavy particles, i.e., without neutral atoms),

$$f_Q = \frac{n_Q}{\sum_{Q'=1}^{Q'_{\max}} n_{Q'}} \times 100\% \tag{7}$$

to allow comparison with experimental results. Additionally, the amount of neutral atoms is given as

$$f_0 = \frac{n_0}{\sum_{Q=0}^{Q_{\max}} n_Q} \times 100\%, \tag{8}$$

which is the percentage of the total heavy particle density

$$n_h = \sum_{Q=0}^{Q_{\max}} n_Q . \tag{9}$$

The mean ion charge state is defined by

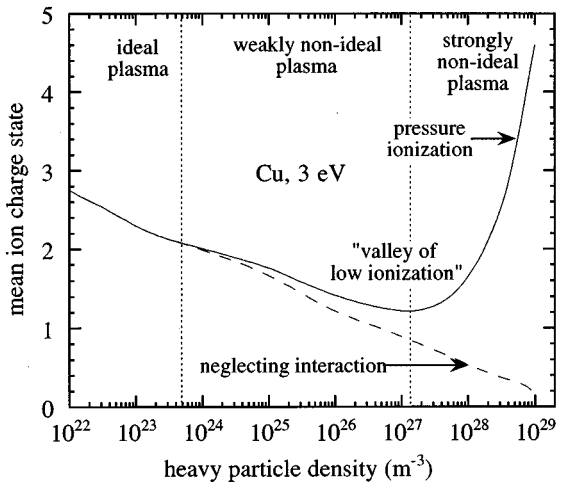

FIG. 2. Mean charge state of copper ions as a function of the heavy particle density at a constant temperature of 3 eV: solid line, particle interaction is taken into account (nonideal plasma); broken line, particle interaction is neglected ($\Delta E_Q \equiv 0$ for all charge states Q).

$$\overline{Q} = \sum_{Q=1}^{Q_{\max}} Q n_Q \Big/ \sum_{Q=1}^{Q_{\max}} n_Q . \tag{10}$$

IV. CALCULATION OF CHARGE STATE DISTRIBUTIONS AT LOW CURRENT, WITHOUT MAGNETIC FIELD

The CSD of the dense, nonideal cathode spot plasma is largely determined by pressure ionization. However, this effect becomes less important when the plasma density decreases due to expansion and the mean ion charge goes through a ''valley of low ionization'' (Fig. 2). The mean ion charge state would increase with decreasing density (i.e., increasing distance from the cathode spot center) if the temperature was constant and equilibrium calculations were applicable. It was experimentally found that the CSDs do not depend on the distance from the spot center and therefore the plasma is in nonequilibrium [31,32,34,35]. Inelastic collisions between heavy particles (ions and atoms) and free electrons are infrequent at large distances (''large'' is here a length of order 100 μm or more [28]). The plasma is not able to relax to its equilibrium state, i.e., the hypothetical equilibrium state changes faster than the plasma can respond and thus the CSD remains almost constant (it is frozen). In contrast, the plasma density in the vicinity of the cathode spot is very high and collisions are sufficiently frequent so as to establish an equilibrium CSD as described by the Saha equations. The transition from equilibrium (dense plasma close to the cathode spot) to nonequilibrium (expanded plasma far from the spot) can be quantified by the Damköhler number, which is defined as the ratio of a characteristic flow time and a characteristic time of nonelastic collisions leading to ionization or recombination. This has been done, for instance, in [31] for a copper plasma. The results suggest that freezing does not happen instantaneously but over a narrow range of plasma density and if a constant temperature is assumed. Freezing occurs at the low-density side of the valley of low

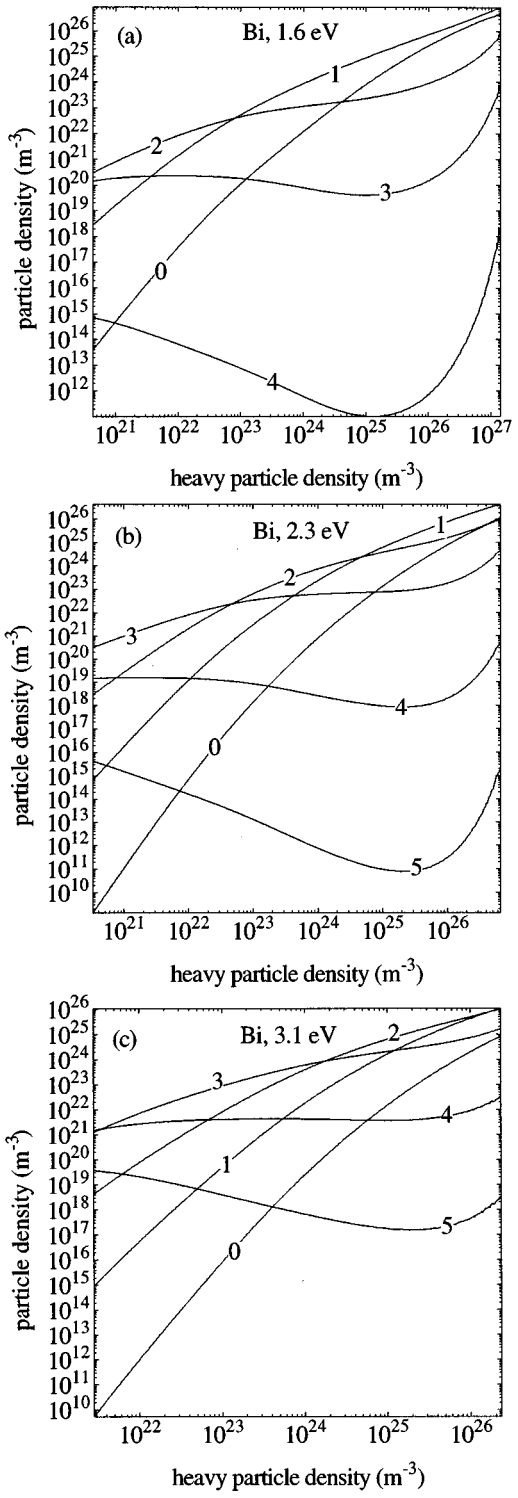

FIG. 3. Example of Saha calculations in the Debye-Hückel approximation. Equilibrium plasma composition for a bismuth plasma at (a) 1.6 eV, (b) 2.3 eV, and (c) 3.1 eV. The numbers indicate the ion charge state.

ionization (Fig. 2) where nonideal plasma effects play only a minor role for the final CSD. Therefore, the use of the relatively simple Debye-Hückel model is justified for this work.

The system of equations (1)–(6) has been solved numerically for all metallic elements as well as for the semimetal carbon and the semiconductors boron, silicon, and germanium. Ionization energies were taken from [54]. In cases where data were missing in [54], theoretical values given by Carlson *et al.* [55] have been used. The latter data have been obtained by self-consistent-field Hartree-Fock calculations that differ in some cases from the data in [54] by more than 20%. Table II shows the ionization energies actually used in the present calculations. Temperature-dependent partition functions have been tabulated for 13 cathode elements (C, Al, Ti, Cr, Fe, Co, Ni, Cu, Zn, Zr, Mo, Ag, and Pb) in [54] by Drawin and Felenbok [50]. Because the ratio of the partition functions were used in the system of Saha equations and not the partition functions themselves, their absolute values are not important for the final results. Moreover, the partition function have only a small effect compared to the exponential dependence on temperature and ionization energy; see Eq. (1). Therefore, the use of constant average values (Table III) for all other elements is acceptable.

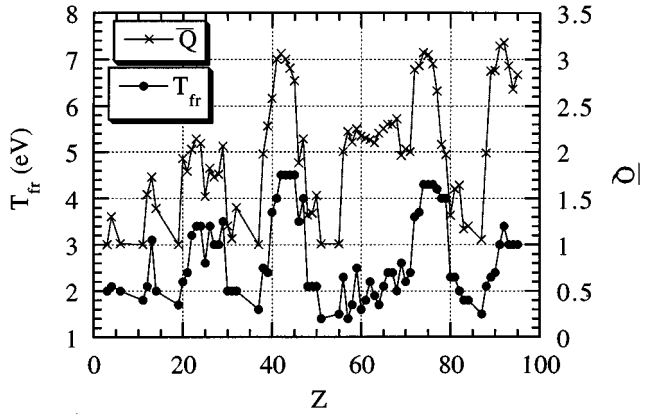

FIG. 4. Freezing temperature and mean ion charge state vs the nuclear charge number of the elements (the connecting lines do not have a physical meaning: they are drawn to guide the eye).

The calculations of plasma compositions (i.e., CSDs) were started for the 13 elements with variable, tabulated partition functions. The following scheme was used to calculate the CSD at a preset electron temperature and density. An initial neutral atom density was assumed and the set of Saha equations was solved, resulting in a ''temporary'' electron density that usually was different from the present electron

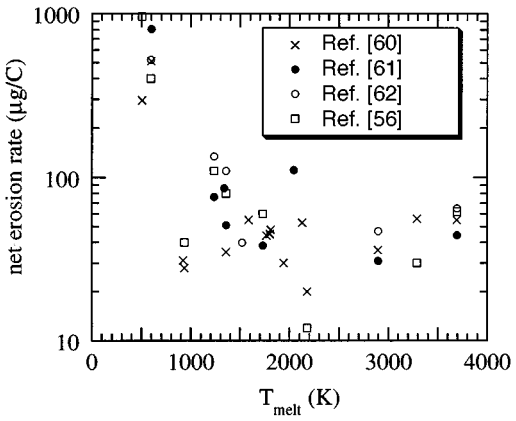

FIG. 5. Experimental net erosion rates vs melting temperature for various elements (data are from Refs. [56,60–62]).

TABLE II. Ionization energies (eV) actually used in the calculations [54,55].

Z	Element	E_0 (eV)	E_1 (eV)	E_2 (eV)	E_3 (eV)	E_4 (eV)	E_5 (eV)	E_6 (eV)	E_7 (eV)
3	Li	5.39	75.64	122.4					
4	Be	9.32	18.21	153.9	217.7				
5	B	8.30	25.16	37.93	259.4	340.2			
6	C	11.3	24.38	47.89	64.49	392.1	490.0		
11	Na	5.14	47.29	71.62	98.91	138.4	172.2	208.5	264.3
12	Mg	7.65	15.04	80.14	109.3	141.3	186.8	225.0	266.0
13	Al	5.99	18.83	28.45	120.0	153.8	190.5	241.8	284.7
14	Si	8.15	16.35	33.49	45.14	166.8	205.3	246.5	303.5
19	K	4.34	31.63	45.81	60.91	82.66	99.40	117.6	154.9
20	Ca	6.11	11.87	50.91	67.27	84.50	108.8	127.2	147.2
21	Sc	6.56	12.80	24.76	73.49	91.65	110.7	138.0	158.1
22	Ti	6.83	13.76	27.49	43.27	99.30	119.5	140.8	170.4
23	V	6.75	14.66	29.31	46.71	65.28	128.1	150.6	173.4
24	Cr	6.77	16.49	30.96	49.16	69.46	90.63	160.2	184.7
25	Mn	7.43	15.64	33.67	51.20	72.40	95.60	119.2	194.5
26	Fe	7.90	16.19	30.65	54.80	75.00	99.10	125.0	151.1
27	Co	7.88	17.08	33.50	51.30	79.50	102.0	128.9	157.8
28	Ni	7.64	18.17	35.19	54.90	76.06	108.0	133.0	162.0
29	Cu	7.73	20.29	36.84	57.38	79.80	103.0	139.0	166.0
30	Zn	9.39	17.96	39.72	59.40	82.60	108.0	134.0	174.0
31	Ga	6.00	20.51	30.71	61.65	95.94	130.2	164.5	198.8
32	Ge	7.90	15.93	34.22	45.71	93.50	124.5	162.0	199.5
37	Rb	4.18	27.28	40.00	52.60	71.00	84.40	99.20	136.0
38	Sr	5.69	11.03	42.89	57.00	71.60	90.80	106.0	122.3
39	Y	6.22	12.24	20.52	60.60	77.00	93.00	116.0	129.0
40	Zr	6.63	13.13	22.99	34.34	80.35	98.00	117.7	137.4
41	Nb	6.76	14.32	25.04	38.30	50.55	102.1	125.0	141.0
42	Mo	7.09	16.16	27.13	46.40	54.49	68.83	125.7	143.6
43	Tc	7.28	15.26	29.54	42.22	57.87	73.51	90.14	106.1
44	Ru	7.36	16.76	28.47	49.90	66.89	83.51	100.1	116.7
45	Rh	7.46	18.08	31.06	53.52	70.90	88.99	106.7	124.4
46	Pd	8.34	19.43	32.93	60.87	78.25	95.64	113.6	131.4
47	Ag	7.58	21.49	34.83	60.52	80.01	99.50	119.0	139.2
48	Cd	8.99	16.91	37.48	58.26	79.62	101.0	122.3	143.7
49	In	5.79	18.87	28.03	54.33	77.51	100.7	123.9	147.1
50	Sn	7.34	14.63	30.50	40.74	72.28	98.67	123.5	148.4
51	Sb	8.64	16.53	25.30	44.20	56.00	108.0	121.7	148.2
55	Cs	3.89	23.16	35.25	48.09	60.93	75.61	89.02	118.3
56	Ba	5.21	10.00	34.45	48.40	62.35	76.30	92.53	107.1
57	La	5.58	11.06	19.18	49.95	61.60	78.28	93.12	111.2
58	Ce	5.54	10.85	20.20	36.76	65.55	80.06	95.24	110.4
59	Pr	5.46	10.55	21.62	38.98	57.53	82.22	97.20	112.2
60	Nd	5.53	10.73	22.10	40.40	68.53	83.81	99.09	114.4
61	Pm	5.55	10.90	22.30	41.10	69.75	85.32	100.9	116.4
62	Sm	5.64	11.07	23.40	41.40	70.93	86.76	102.6	118.4
63	Eu	5.67	11.24	24.92	24.92	42.70	72.33	88.47	104.6
64	Gd	6.15	12.09	20.63	44.00	71.99	88.91	105.8	122.7
65	Tb	5.86	11.52	21.91	39.79	73.14	90.35	107.6	124.8
66	Dy	5.94	11.67	22.80	41.40	76.28	93.26	110.3	127.2
67	Ho	6.02	11.80	22.84	42.50	77.53	94.79	112.1	129.3
68	Er	6.11	11.93	22.74	42.70	78.76	96.29	113.8	131.4
69	Tm	6.18	12.05	23.68	42.70	79.98	97.77	115.6	133.4
70	Yb	6.25	12.18	25.05	43.56	81.18	99.24	117.3	135.4
71	Lu	5.43	13.90	20.96	45.25	66.80	98.42	117.3	136.2

TABLE II. (*Continued*).

Z	Element	E_0 (eV)	E_1 (eV)	E_2 (eV)	E_3 (eV)	E_4 (eV)	E_5 (eV)	E_6 (eV)	E_7 (eV)
72	Hf	6.82	14.90	23.30	33.33	67.82	98.23	117.9	137.5
73	Ta	7.89	14.47	23.49	36.32	49.14	92.66	118.7	139.1
74	W	7.98	15.08	25.43	39.29	53.15	67.01	119.7	140.8
75	Re	7.88	15.73	25.89	41.49	56.33	71.17	86.01	142.9
76	Os	8.70	16.34	27.71	42.70	59.29	75.04	90.80	106.5
77	Ir	9.10	16.91	29.50	45.33	61.16	78.70	95.32	111.9
78	Pt	9.00	19.24	35.25	51.27	67.28	83.29	101.0	117.9
79	Au	9.23	20.50	37.37	54.80	70.99	87.81	104.6	123.2
80	Hg	10.4	18.76	34.20	52.93	71.09	89.24	107.4	125.6
81	Tl	6.11	20.43	29.83	50.17	69.70	89.23	108.8	128.3
82	Pb	7.42	15.03	31.94	42.32	68.80	87.98	108.7	129.5
83	Bi	7.29	16.69	26.85	46.06	58.16	85.78	107.7	129.6
84	Po	8.42	17.18	29.01	39.58	61.26	74.08	105.7	128.7
87	Fr	3.61	20.02	31.63	43.25	54.87	71.74	84.94	114.2
88	Ra	5.28	10.15	30.97	43.49	56.02	68.55	87.42	101.6
89	Ac	5.17	12.10	16.93	43.36	56.66	69.95	83.25	104.3
90	Th	6.08	11.50	20.00	28.80	57.22	71.21	85.20	99.18
91	Pa	5.89	11.46	17.75	28.91	46.69	74.36	88.37	102.4
92	U	6.19	11.63	18.09	30.90	49.91	68.91	90.35	104.7
93	Np	6.27	11.80	18.37	32.75	52.83	72.91	92.14	106.7
94	Pu	6.06	11.19	20.70	40.80	60.90	80.40	94.89	109.4
95	Am	5.99	12.15	18.82	36.15	58.14	80.12	95.31	110.4

density. The assumed neutral density was then varied to minimize the difference between the preset and calculated electron density until a self-consistent CSD was obtained. The calculation was continued with the same temperature at the next preset electron density. The calculation was stopped at high densities when the lowering of the ionization energy approaches the ionization energy. This is the region of strongly nonideal plasma where the Debye-Hückel theory is not valid anymore. The next step was to compare calculated with experimental CSD data. The experimental mean ion charge state Q_{expt} was taken from Table I and the mean ion charge state closest to Q_{expt} was identified for the given temperature. This closest value was labeled Q_{calc} and the CSD associated with Q_{calc} was compared with the experimental CSD associated with Q_{expt}. Usually they did not match. The whole procedure was repeated for a different preset temperature. It turned out that the calculated CSD becomes broader at higher temperatures for a given Q_{expt}. This feature allows us to repeat the calculations with higher or lower temperature for a too narrow or a too broad calculated CSD, respectively, until the calculated and experimental CSDs become similar. There is of course no guarantee that they will indeed become similar because the assumptions underlying the calculations might not be valid. However, the procedure was successful in most cases in the sense that the measured CSDs could be reproduced by the calculations.

TABLE III. Constant partition functions used for most calculations; the data are average values of the data for C, Al, Ti, Cr, Fe, Co, Ni, Cu, Zn, Zr, Mo, Ag, and Pb taken from the handbook by Drawin and Felenbok [50] at the effective freezing parameters for each element.

Ion charge state	Partition function
0	280
1	150
2	45
3	15
4	12
5	6
6	1

As an example for the calculations, Fig. 3 shows the equilibrium plasma composition of a bismuth plasma at three different temperatures [(a) 1.6 eV, (b) 2.3 eV, and (c) 3.1 eV]. All results are conveniently presented in the form of a ''periodic table of vacuum arc CSD'' (Table IV). Percentages of neutral atoms appear in Table IV, but are written in parentheses to distinguish them from ion particle fraction [note the difference in definitions Eqs. (7) and (8)]. The calculated density of neutral atoms is the result of ionization and recombination reaction under equilibrium conditions; it does not include the enhancement due to evaporating macroparticles and evaporation from hot, liquid metal pools of previously active craters.

V. CALCULATION OF CHARGE STATE DISTRIBUTIONS AT HIGH CURRENT AND WITH MAGNETIC FIELD

As mentioned in the Introduction, ion charge states can be enhanced by external magnetic field and high discharge currents. The most comprehensive experimental study was done by Oks *et al.* [19,25] and their results have been included in Table V. Oks *et al.* argue that a high discharge current is

TABLE IV. Periodic table of calculated vacuum arc CSD. The KEY indicates the order of data; the mean ion charge state is underlined; the particle percentages are defined by Eqs. (7) and (8); and the densities and temperature at the CSD freezing point are given in m^{-3} and eV, respectively. The notation $4.2[-2]=4.2\times10^{-2}$. The symbols of ''new'' (not yet experimentally investigated) elements are written in *italics*. The last line in each element box shows comments: !, very good agreement of calculated with experimental CSD data; VP, calculation done with variable partition function (if not stated, the constant partition functions of Table III have been used); B, experimental CSD is substantially broadened; U, uncertain temperature and density at freezing (due to relative insensitivity of CSD on temperature and density); and N, ''new'' element, i.e., experimental CSD not known.

1 H								
3 Li 1.00 (0: 1.5 [-2]) 1: 100. 0 2: 2 [-13] 3: 0 4: 0 n_e= 1.0 [23] n_h= 1.0 [23] T= 2.0; !, U	**4 *Be*** 1.30 (0: 1.5) 1: 70.0 2: 30.0 3: 0 4: 0 n_e= 3.1 [24] n_h= 2.4 [24] T= 2.1; N							
11 *Na* 1.00 (0: 2.2 [-2]) 1: 100.0 2: 1.8 [-5] 3: 0 4: 0 n_e= 1.0 [23] n_h= 1.0 [23] T= 1.8; N	**12 Mg** 1.54 (0: 0.82) 1: 46.0 2: 54.0 3: 3.1 [-15] 4: 0 n_e= 6.0 [24] n_h= 3.9 [24] T= 2.1; !, U							
19 *K* 1.00 (0: 1.7 [-2]) 1: 99.9 2: 0.1 3: 3.5 [-9] 4: 0 n_e= 1.0 [23] n_h= 1.0 [23] T= 1.7; N	**20 Ca** 1.93 (0: 2.6 [-2]) 1: 7.0 2: 93.0 3: 3.2 [-5] 4: 0 n_e= 2.9 [24] n_h= 1.5 [24] T= 2.2	**21 Sc** 1.79 (0: 0.47) 1: 23.6 2: 73.7 3: 2.7 4: 5.4 [-10] n_e= 2.4 [25] n_h=1.3 [25] T= 2.4	**22 Ti** 2.03 (0: 4.2 [-2]) 1: 9.8 2: 78.0 3: 12.3 4: 8.8 [-3] n_e= 1.7 [25] n_h= 8.2 [24] T= 3.2; VP	**23 V** 2.14 (0: 0.37) 1: 5.5 2: 75.0 3: 19.5 4: 3.8 [-2] n_e= 1.7 [25] n_h= 8.1 [24] T= 3.4	**24 Cr** 2.09 (0: 3.7 [-2]) 1: 9.6 2: 71.8 3: 18.6 4: 5.6 [-2] n_e= 2.0 [25] n_h= 9.6 [24] T= 3.4; VP	**25 Mn** 1.52 (0: 1.3) 1: 48.0 2: 51.9 3: 0.1 4: 8.7 [-7] n_e= 4.5 [25] n_h= 3.0 [25] T= 2.6	**26 Fe** 1.82 (0: 0.37) 1: 24.1 2: 69.7 3: 6.2 4: 3.2 [-3] n_e= 4.4 [25] n_h= 2.4 [25] T=3.4; !, VP	**27 Co** 1.73 (0: 0.78) 1: 27.9 2: 71.7 3: 0.44 4: 4.7 [-5] n_e= 2.5 [25] n_h= 1.4 [25] T= 3.0; VP,B
37 *Rb* 1.00 (0: 2.0 [-2]) 1: 99.8 2: 0.2 3: 9.7 [-8] 4: 0 5: 0 6: 0 n_e= 1.0 [23] n_h= 1.0 [23] T= 1.6; N	**38 Sr** 1.98 (0: 3.1 [-3]) 1: 2.0 2: 98.0 3:1.8 [-3] 4: 0 5: 0 6: 0 n_e= 2.3 [24] n_h=1.2 [24] T= 2.5; !,U	**39 Y** 2.28 (0: 2.3 [-2]) 1: 5.1 2: 62.0 3: 32.9 4: 2.9 [-6] 5: 0 6: 0 n_e= 5.2 [24] n_h= 2.3 [24] T= 2.4; !	**40 Zr** 2.58 (0: 6.1 [-3]) 1: 1.5 2: 46.3 3: 45.0 4: 7.2 5: 1.7 [-5] 6: 0 n_e= 2.2 [25] n_h= 8.4 [24] T= 3.7; !,VP	**41 Nb** 3.00 (0: 1.9 [-3]) 1: 0.6 2: 19.4 3: 59.9 4: 19.8 5: 0.24 6: 1.8 [-9] n_e= 1.9 [25] n_h= 6.2 [24] T= 4.0; B	**42 Mo** 3.06 (0: 4.1 [-4]) 1: 0.2 2: 7.7 3: 78.4 4: 13.6 5: 8.4 [-2] 6: 3.4 [-5] n_e=1.8 [25] n_h= 6.0 [24] T= 4.5; VP,B	**43 *Tc*** 3.00 (0: 6.6 [-4]) 1: 0.35 2: 19.6 3: 60.0 4: 19.9 5: 0.13 6: 8.1 [-6] n_e= 1.4 [25] n_h= 4.6 [24] T= 4.5; N	**44 *Ru*** 2.90 (0: 6.1 [-4]) 1: 0.36 2: 16.9 3: 74.9 4: 7.8 5: 1.3 [-2] 6: 2.2 [-7] n_e= 1.2 [25] n_h= 4.0 [24] T= 4.5; N	**45 *Rh*** 2.77 (0: 9.5 [-3]) 1: 0.64 2: 25.3 3: 70.4 4: 3.6 5: 2.8 [-3] 6: 1.4 [-8] n_e= 1.0 [25] n_h= 3.6 [24] T= 4.5; N
55 *Cs* 1.01 (0: 2.1 [-2]) 1: 99.2 2: 0.7 3: 1.8 [-6] 4: 0 5: 0 6: 0 n_e= 1.0 [23] n_h= 1.0 [23] T= 1.5; N	**56 Ba** 2.00 (0: 2.1 [-3]) 1: 0.54 2: 98.9 3: 0.52 4: 1.6 [-5] 5: 0 6: 0 n_e= 5.1 [23] n_h= 2.5 [23] T= 2.3; !, U	**57 La*** 2.22 (0: 1.1 [-4]) 1: 0.88 2: 76.2 3: 22.9 4: 5.0 [-12] 5: 0 6: 0 n_e= 1.4 [22] n_h= 6.1 [21] T= 1.4; !, U	**72 Hf** 2.89 (0: 0.011) 1: 2.0 2: 26.6 3: 51.7 4: 19.7 5: 4.2 [-4] 6: 0 n_e= 2.5 [25] n_h= 8.7 [24] T= 3.6; B	**73 Ta** 2.93 (0: 4.7 [-3]) 1: 1.0 2: 21.7 3: 61.1 4: 16.1 5: 0.11 6: 2.2 [-9] n_e= 1.7 [25] n_h= 5.9 [24] T= 3.7; B	**74 W** 3.07 (0: 3.0 [-3]) 1: 0.61 2: 16.8 3: 58.1 4: 24.2 5: 0.32 6: 6.8 [-5] n_e= 2.8 [25] n_h= 9.0 [24] T= 4.3; B	**75 *Re*** 3.05 (0: 1.4 [-3]) 1: 0.44 2: 15.0 3: 63.7 4: 20.7 5: 0.16 6: 1.6 [-5] n_e= 1.8 [25] n_h= 5.8 [24] T= 4.3; N	**76 *Os*** 2.95 (0: 2.2 [-3]) 1: 0.63 2: 20.6 3: 62.2 4: 16.5 5: 6.8 [-2] 6: 2.9 [-6] n_e= 1.6 [25] n_h= 5.3 [24] T= 4.3; N	**77 Ir** 2.66 (0: 7.0 [-3]) 1: 1.6 2: 36.4 3: 56.2 4: 5.8 5: 1.0 [-2] 6: 1.1 [-7] n_e= 1.7 [25] n_h= 6.4 [24] T= 4.2; B
87 *Fr* 1.05 (0: 1.7 [-2]) 1: 94.5 2: 5.5 3: 2.2 [-4] 4: 0 n_e= 9.5 [22] n_h= 1.0 [23] T= 1.5; N	**88 *Ra*** 1.99 (0: 1.4 [-3]) 1: 1.5 2: 98.1 3: 0.4 4: 1.0 [-5] n_e= 8.2 [23] n_h= 4.1 [23] T= 2.1; N	**89*Ac***** 2.87 (0: 1.7 [-4]) 1: 0.27 2: 12.4 3: 87.3 4: 1.67 n_e= 8.6 [23] n_h= 3.0 [23] T= 2.3; N						
		*** Lanthanides**	**58 Ce** 2.11 (0: 2.0 [-3]) 1: 2.5 2: 83.8 3: 13.7 4: 3.4 [-4] n_e= 2.4 [23] n_h= 1.1 [23] T= 1.7; !	**59 Pr** 2.25 (0: 1.2 [-2]) 1: 3.0 2: 69.6 3: 27.4 4: 3.2 [-2] n_e= 7.2 [24] n_h= 3.2 [24] T= 2.5; !	**60 Nd** 2.17 (0: 3.5 [-5]) 1: 0.36 2: 82.1 3: 17.5 4: 1.0 [-5] n_e= 2.1 [22] n_h= 9.4 [21] T= 1.6; !	**61 *Pm*** 2.15 (0: 2.74 [-4]) 1: 0.87 2: 82.8 3: 16.3 4: 2.36 [-4] n_e= 1.2 [23] n_h= 5.5 [22] T= 1.8; N	**62 Sm** 2.13 (0: 2.8 [-3]) 1: 2.1 2: 82.9 3: 15.0 4: 2.1 [-3] n_e= 1.2 [24] n_h= 5.8 [23] T= 2.2; !	**63 *Eu*** 2.10 (0: 1.5 [-4]) 1: 0.65 2: 88.9 3: 10.5 4: 2.7 [-4] n_e= 1.0 [23] n_h= 4.9 [22] T= 1.9; N
		**** Actinides**	**90 Th** 2.88 (0: 2.5 [-7]) 1: 0.3 2: 23.4 3: 64. 3 4: 12.0 5: 1.1 [-5] 6: 0 n_e= 8.7 [23] n_h= 3.0 [23] T= 2.4; !	**91 *Pa*** 3.14 (0: 1.2 [-3]) 1: 0.34 2: 11.0 3: 61.6 4: 25.6 5: 2.3 [-2] 6: 8.4 [-10] n_e= 1.0 [25] n_h= 3.3 [24] T= 3.0; N	**92 U** 3.18 (0: 1.95 [-3]) 1: 0.35 2: 9.7 3: 60.9 4: 29.0 5: 0.04 6: 8.9 [-7] n_e= 2.5 [25] n_h= 7.9 [24] T= 3.4	**93 *Np*** 2.93 (0: 1.6 [-3]) 1: 0.48 2: 15.2 3: 75.1 4: 9.2 5: 1.1 [-3] 6: 6.6 [-11] n_e= 8.9 [24] n_h= 3.0 [24] T= 3.0; N	**94 *Pu*** 2.68 (0: 2.7 [-3]) 1: 0.8 2: 31.0 3: 67.6 4: 0.54 5: 4.1 [-6] 6: 0 n_e= 9.2 [24] n_h= 3.4 [24] T= 3.0; N	**95 *Am*** 2.83 (0: 2.05 [-3]) 1: 0.66 2: 18.5 3: 77.8 4: 3.0 5: 6.0 [-5] 6: 0 n_e= 9.0 [24] n_h= 3.2 [24] T= 3.0; N

KEY

element number, name
(neutral (% of n_h))
onefold (%)
twofold (%)
threefold (%)
fourfold (%)
electron density (m^{-3})
heavy particle density (m^{-3})
temperature (eV)

22 Ti 2.03 ← mean ion charge
(0: 4.2 [-2])
1: 9.8
2: 78.0
3: 12.3
4: 8.8 [-3]
n_e= 1.7 [25]
n_h= 8.2 [24]
T= 3.2; VP ← comment

notation
4.2 [-2] = 4.2 x 10^{-2}

TABLE IV. (*Continued*).

							2 He
			5 *B* 1.01 (0: 2.3) 1: 99.4 2: 0.6 3: 9.3 [-6] 4: 0 n_e= 4.0 [24] n_h= 4.0 [24] T= 2.0; N	6 C 1.00 (0: 3.52) 1: 99.7 2: 0.30 3: 5.1 [-8] 4: 0 n_e= 1.6 [25] n_h= 1.0 [25] T= 2.0; !, U	7 N	8 O	9 F	10 Ne
			13 Al 1.73 (0: 0.14) 1: 36.2 2: 54.4 3: 9.5 4: 3.3 [-15] n_e= 1.4 [25] n_h= 8.2 [24] T= 3.1; !,VP	14 Si 1.39 (0: 1.1) 1: 60.8 2: 39.2 3: 6.5 [-3] 4: 0 n_e= 3.3 [24] n_h= 2.4 [24] T= 2.0; B	15 P	16 S	17 Cl	18 Ar
28 Ni 1.76 (0: 0.59) 1: 24.5 2: 74.7 3: 0.77 4: 3.5 [-5] n_e= 1.5 [25] n_h= 8.8 [24] T= 3.0; VP,B	29 Cu 2.06 (0: 3.0 [-2]) 1: 10.7 2: 72.1 3: 17.1 4: 1.4 [-2] n_e= 4.8 [24] n_h= 2.3 [24] T= 3.5; VP,B	30 Zn 1.20 (0: 8.3) 1: 80.0 2: 20.0 3: 3 [-4] 4: 0 n_e= 5.9 [24] n_h= 5.4 [24] T=2.0; !,VP,U	31 *Ga* 1.06 (0: 0.67) 1: 93.7 2: 6.3 3: 3.5 [-3] 4: 0 n_e= 3.9 [24] n_h= 3.7 [24] T= 2.0; N	32 Ge 1.40 (0: 1.8) 1: 59.6 2: 40.4 3: 4.0 [-5] 4: 3.8 [-9] n_e= 4.0 [24] n_h= 2.9 [24] T= 2.0; !, U	33 As	34 Se	35 Br	36 Kr
46 Pd 1.88 (0: 0.16) 1: 19.7 2: 72.3 3: 7.8 4: 8.5 [-4] 5: 5.3 [-10] 6: 0 n_e= 2.0 [25] n_h= 1.0 [25] T= 3.5; B	47 Ag 2.14 (0: 5.7 [-2]) 1: 3.8 2: 78.5 3: 17.6 4: 0.012 5: 6.6 [-8] 6: 0 n_e= 2.8 [25] n_h= 1.3 [25] T= 4.0; VP,B	48 Cd 1.32 (0: 2.3) 1: 68.0 2: 32.0 3: 1.2 [-3] 4: 0 5: 0 6: 0 n_e= 6.0 [24] n_h= 4.6 [24] T= 2.1; !,U	49 In 1.34 (0: 2.0) 1: 66.0 2: 34.0 3: 1.3 [-3] 4: 0 5: 0 6: 0 n_e= 5.3 [24] n_h= 4.0 [24] T= 2.1; !, U	50 Sn 1.53 (0: 1.0) 1: 47.0 2: 53.0 3: 4.6 [-2] 4: 0 5: 0 6: 0 n_e= 8.3 [24] n_h= 5.4 [24] T= 2.1; !, U	51 Sb 1.01 (0: 26.9) 1: 99.2 2: 0.8 3: 1.47 [-5] 4: 0 5: 0 6: 0 n_e= 6.3 [24] n_h= 8.6 [23] T= 1.4; !, U	52 Te	53 I	54 Xe
78 Pt 2.08 (0: 5.0 [-2]) 1: 7.8 2: 76.4 3: 15.6 4: 0.17 5: 2.5 [-5] 6: 0 n_e= 2.1 [25] n_h= 1.0 [25] T= 4.0; B	79 Au 1.97 (0: 8.2 [-2]) 1: 12.5 2: 77.8 3: 9.6 4: 5.1 [-2] 5: 3.0 [-6] 6: 0 n_e= 2.0 [25] n_h= 1.0 [25] T= 4.0; !	80 *Hg* 1.32 (0: 2.7) 1: 68.5 2: 31.5 3: 2.4 [-2] 4: 1.6 [-8] 5: 0 6: 0 n_e= 6.0 [24] n_h= 4.7 [24] T= 2.3; N	81 *Tl* 1.60 (0: 0.28) 1: 41.6 2: 56.8 3: 1.6 4: 4.9 [-4] 5: 0 6: 0 n_e= 7.5 [23] n_h= 4.7 [23] T= 2.3; N	82 Pb 1.64 (0: 0.51) 1: 36.3 2: 63.5 3: 0.22 4: 1.3 [-6] 5: 0 6: 0 n_e= 1.6 [24] n_h= 9.9 [23] T= 2.0; !, U	83 Bi 1.17 (0: 1.4) 1: 83.0 2: 16.9 3: 3.4 [-2] 4: 4.3 [-7] 5: 0 6: 0 n_e= 3.1 [24] n_h= 2.7 [24] T= 1.8; !, U	84 *Po* 1.20 (0: 1.6) 1: 79.8 2: 20.2 3: 9.2 [-3] 4: 0 5: 0 6: 0 n_e= 1.7 [24] n_h= 1.4 [24] T= 1.8; N	85 At	86 Rn

64 Gd 2.20 (0: 1.0 [-3]) 1: 2.1 2:76.4 3: 21.5 4: 1.6 [-4] n_e= 9.9 [22] n_h= 4.5 [22] T= 1.7	65 *Tb* 2.25 (0: 1.56 [-3]) 1: 1.6 2: 71.5 3: 26.8 4: 5.3 [-3] n_e= 6.3 [23] n_h= 2.8 [23] T= 2.1; N	66 Dy 2.30 (0: 2.5 [-3]) 1: 1.7 2: 66.5 3: 31.8 4: 1.8 [-2] n_e= 1.7 [24] n_h=7.4 [23] T= 2.4; !	67 Ho 2.30 (0: 2.6 [-3]) 1: 1.8 2: 66.4 3: 31.8 4: 1.2 [-2] n_e= 1.7 [24] n_h= 7.2 [23] T= 2.4; !	68 Er 2.36 (0: 1.6 [-4]) 1: 0.57 2: 63.0 3: 36.4 4: 2.5 [-3] n_e= 1.3 [23] n_h= 5.5 [22] T= 2.0	69 Tm 1.96 (0: 0.19) 1: 12.9 2: 77.9 3: 9.0 4: 2.5 [-3] n_e= 2.8 [25] n_h= 1.4 [25] T= 2.6; !	70 Yb 2.03 (0: 7.6 [-3]) 1: 4.0 2: 88.9 3: 7.1 4: 3.4 [-4] n_e= 1.3 [24] n_h= 6.6 [23] T= 2.2; !	71 *Lu* 2.00 (0: 0.11) 1: 17.2 2: 64.1 3: 18.2 4: 6.6 [-4] n_e= 1.0 [25] n_h= 5.1 [24] T= 2.0; N
96 *Cm*	97 *Bk*	98 *Cf*	99 *Es*	100 *Fm*	101 *Md*	102 *No*	103 *Lr*

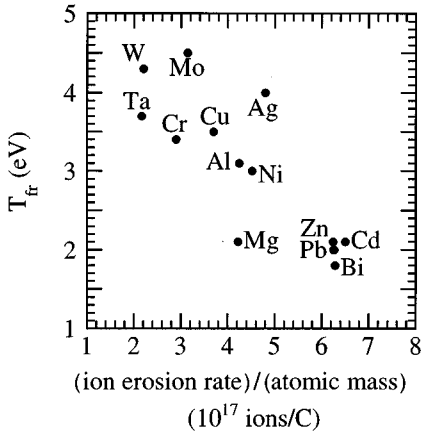

FIG. 6. Freezing temperature vs ion erosion rate (ion erosion data from [56,62] are normalized by ion mass).

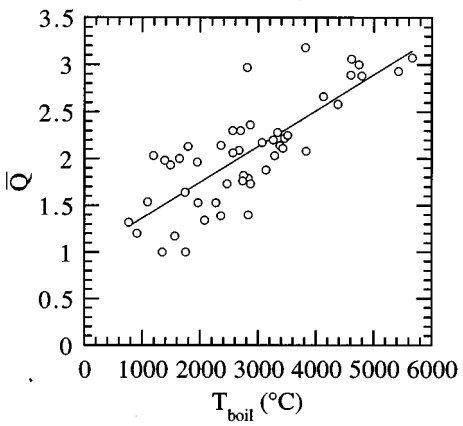

FIG. 7. Statistical correlation of the mean ion charge state and boiling temperature [the best linear fit (without carbon) is $Q = 0.98 + 3.8 \times 10^{-4} T_{boil}$, with T_{boil} in °C].

necessarily associated with a magnetic self-field and therefore the results with an external magnetic field and at high current are similar.

Saha calculations in Debye-Hückel approximation were performed to identify the freezing parameters (effective temperature and density at the CSD freezing point) valid for their experimental conditions. The results of these calculations are included in Table V. Use of a magnetic field causes greater deviations between experimental and calculated CSDs.

VI. DISCUSSION

A. CSDs at low current

The close agreement of many experimental CSD (Table I) with the theoretical values (Table IV) justifies the assumptions made: (i) the spot plasma experiences an almost instantaneous transition from equilibrium to nonequilibrium while expanding and (ii) the plasma parameters at the freezing point fluctuate only marginally allowing determination of an average effective freezing temperature and an effective freezing density for most elements.

There are two ''problematic'' groups of cathode elements. One group of elements has the problem that their CSD is dominated by only one or two charge states (for instance, Li, C, Zn, Sr, Cd, Sn, Sb, Ba, and Pb). This results in a large uncertainty of the calculated effective temperature (± 0.5 eV) and density at freezing ($\pm$ order of magnitude or even more) because the CSDs of these elements are relatively insensitive to variations of temperature and density. This has been marked with a U (denoting uncertain) in Table IV.

The other problematic group includes Mo, Ag, Hf, Ta, W, and Ir. The experimentally observed CSDs are substantially broader than the calculated [marked with B (denoting broadened CSD) in Table IV]. The assumptions are obviously not well justified for these elements.

It is known that the experimental CSDs have been determined by averaging over many individual discharges. The cathode spots are of nonstationary nature and a CSD measured at a certain instant of time and for an individual pulsed discharge differs from a CSD measured at a different time or discharge even when the macroscopic conditions are kept constant. For instance, Figs. 4–6 of Ref. [18] show that CSDs scatter when individually measured for a 200-ns window 100 μs after discharge triggering. The scattering of individual CSDs suggests that the plasma parameters fluctuate, a well-known phenomena of vacuum arcs. Therefore, it must be expected that experimentally determined, average CSDs are broader than the CSDs calculated with a single effective temperature and effective density at freezing. The present calculations suggest that this broadening mechanism is particularly pronounced for the problematic elements Mo, Ag, Hf, Ta, W, and Ir.

Another explanation is that the assumption of instantaneous freezing is a bad approximation for these elements, i.e., freezing of charge states does not happen instantaneously. At least one of the broadening effects is particularly strong for refractory metals, and more work is needed to clarify this problem by measuring the scatter between individual CSDs for the different elements.

The effective plasma temperature at the freezing point is correlated to the mean ion charge (Fig. 4), a consequence of the exponential temperature dependence of ionization events. An interesting question is why some materials have a higher effective freezing temperature than others. The plasma temperature results from the energy balance, which is greatly influenced by the energy input per plasma volume. For a given power input (discharge current times cathode voltage drop) one can assume that the amount of plasma produced decreases with increasing melting temperature because more energy must be invested in heating the future cathode crater volume before the solid is transferred into plasma. On the other hand, low-melting-point materials produce more droplets and less energy remains for the plasma. An analysis of available literature data shows that the net erosion rate statistically does not depend on the melting temperature, with the exception of materials with very low melting point (such as Pb, Sn, and Cd); see Fig. 5. Daalder [56] pointed out that the erosion rate is not constant but increases with charge transferred, and the compiled data are valid for about 10 C. The situation becomes clearer by considering the *ion* erosion rate (cathode mass loss in the form of ions is normalized by the charge transferred). Figure 6 shows that the higher the ion erosion rate (normalized by the mass to obtain ion num-

TABLE V. Charge state distributions and mean ion charge states for vacuum arcs in a magnetic field (B_{max}=375 mT, I_{arc}=220 A, experimental data are from Ref. [19], theoretical values are from this work, and comments are the same as in Table IV). The notation 2.7[24]=2.7×10^{24}.

Experiments													Calculation						
Z	Element	$\overline{Q^B_{expt}}$	f_1 (%)	f_2 (%)	f_3 (%)	f_4 (%)	f_5 (%)	f_6 (%)	$n_{e,fr}$ (m^{-3})	$n_{h,fr}$ (m^{-3})	T_{fr} (eV)	(f_0) (%)	f_1 (%)	f_2 (%)	f_3 (%)	f_4 (%)	f_5 (%)	f_6 (%)	Comments
6	C	1.40	60	40					2.7[24]	1.9[24]	3.0	0.94	59.1	40.8	7.0[−2]				!,VP,U
12	Mg	1.95	5	95					4.5[24]	2.3[24]	3.0	1.5[−2]	5.2	94.8	8.3[−7]				!
13	Al	2.40	10	40	50				1.1[25]	4.5[24]	4.0	2.8[−2]	9.9	40.0	50.1	1.5[−7]			!,VP
21	Sc	2.47	16	23	59	2			2.5[25]	9.9[24]	3.5	1.3[−2]	2.3	48.3	49.3	1.4[−4]			B
22	Ti	2.61	5	35	54	6			1.9[25]	7.1[24]	4.5	7.6[−4]	1.2	38.9	57.8	2.2	1.7[−7]		VP
23	V	2.51	13	31	48	8			1.7[25]	6.8[24]	4.0	4.3[−3]	1.5	46.7	50.8	0.49	2.9[−4]		B
24	Cr	2.60	11	26	55	8			1.1[25]	4.4[24]	4.0	1.8[−4]	1.4	39.8	56.8	1.9	6.3[−5]		VP
25	Mn	2.03	26	47	25	2			1.5[25]	7.2[24]	3.5	2.4[−2]	6.2	84.7	9.1	1.9[−2]	7.0[−8]		B
26	Fe	2.28	7	58	35				2.0[25]	8.9[24]	4.0	2.3[−2]	4.5	63.2	32.0	0.28	1.1[−5]		VP
27	Co	2.01	19	62	18	1			1.7[25]	8.6[24]	3.8	2.7[−2]	4.4	90.3	5.33	2.6[−2]	2.4[−8]		VP,B
28	Ni	2.30	9	56	31	4			2.3[25]	9.9[24]	5.0	7.1[−3]	2.6	66.7	28.6	2.2	2.8[−4]		VP
29	Cu	2.48	8	41	47	3	1		1.4[25]	5.5[24]	4.5	1.2[−2]	5.0	42.5	51.7	0.78	1.1[−4]		VP
39	Y	2.87	6	9.0	77	8			2.3[24]	8.0[23]	3.0	1.5[−4]	0.15	12.8	87.0	2.5[−3]			
41	Nb	3.73	1	9.0	23	52	13	2	2.0[25]	5.4[24]	4.9	7.1[−5]	3.7[−2]	2.69	29.2	60.4	7.6	1.0[−5]	B
42	Mo	3.47	5	11	26	48	10		2.5[25]	7.2[24]	5.5	3.8[−5]	2.5[−2]	1.99	50.7	44.6	2.6	1.9[−2]	VP,B
56	Ba	2.60	2	41	53	3	3	1	3.1[23]	1.2[23]	3.3	1.8[−6]	2.4[−2]	43.0	54.4	2.50	1.1[−3]		
57	La	2.98	3	16	61	20			5.6[22]	1.9[22]	2.4	7.2[−8]	1.6[−3]	2.00	98.0	3.2[−2]	2.4[−8]		B
64	Gd	2.70	1	43	41	15			1.2[24]	4.4[23]	2.5	4.7[−4]	0.50	29.3	70.2	3.9[−2]			B
68	Er	3.00	2	12	70	16			2.3[23]	7.3[22]	2.9	6.8[−7]	6.4[−3]	4.6	90.8	4.6	6.1[−7]		B
72	Hf	3.39	5	16	31	32	15	1	2.7[25]	8.0[24]	4.1	1.6[−3]	0.38	9.2	41.2	49.2	1.5[−2]	2.3[−9]	B
73	Ta	4.27	1	5.0	13	40	41	2	2.3[25]	5.4[24]	5.6	4.3[−6]	2.4[−3]	0.26	7.21	58.0	34.6	1.4[−2]	B
74	W	4.17	1	5.0	16	39	32	7	2.1[25]	5.1[24]	5.8	5.4[−6]	3.3[−3]	0.39	9.75	62.7	26.7	0.40	B
78	Pt	2.77	3	25	64	8			1.3[24]	4.6[23]	4.0	1.0[−4]	0.24	28.9	64.3	6.6	7.3[−3]		
82	Pb	2.23	1	75	24				1.2[23]	5.5[22]	2.3	7.2[−4]	1.2	74.7	24.0	2.4[−2]			!
83	Bi	2.22	9	60	31				1.0[25]	4.6[24]	3.1	4.6[−2]	9.1	59.9	30.9	8.1[−2]			!

bers) the lower the plasma temperature at freezing. Figure 6 shows also that elements of low ion erosion rate are elements with high boiling point (and vice versa); this is in agreement with the known statistical correlation (Fig. 7) of mean ion charge state and boiling temperature [21].

B. CSDs at high current or in a magnetic field

The effect of CSD broadening becomes significantly enhanced when operating at high current or with an external magnetic field: the agreement of experimental CSD with calculated CSD (Table V) is not as good as in Sec. IV (Tables I and IV). Significantly broader CSD are observed for Co, Ni, Mo, Hf, Ta, and W. The plasma temperatures at freezing are higher (by about 1 eV). A simple estimate shows that more energy is invested in each plasma particle: The plasma production is approximately proportional to the arc current [57], but the power is more than proportional to the current since the burning voltage increases with current. A higher current therefore causes a higher plasma temperature. A higher current is also associated with the simultaneous existence of several cathode spots and the cathode plasma expansion occurs under the influence of neighboring plasma. The expansion is not as rapid as with a single-spot plasma, and thermodynamic expansion cooling is weaker. A magnetic field has a similar effect: The plasma does not freely expand. The very dense spot plasma is dominated by collisions, but expansion is slower for distances from the cathode spot where the magnetic pressure is of order of or greater than the kinetic pressure, that is, for a characteristic distance [58]

$$d_B \geqslant \frac{1}{B}\sqrt{2\mu_0 \gamma I_{\mathrm{arc}} kT}, \tag{11}$$

where μ_0 is the permeability of vacuum and γ is a constant (10^{13} $\mathrm{A}^{-1}\,\mathrm{m}^{-1}$ for Cu [57]). Slower expansion leads to slower freezing. The assumption of ''instantaneous freezing'' and the concept of an effective freezing temperature and effective freezing density are less suitable. The calculations suggest that either the scattering of individually measured CSDs is greater in the presence of a magnetic field or freezing is not instantaneous. Future measurements of CSD scattering with and without a magnetic field will allow distinguishing between the broadening mechanisms.

VII. PREDICTION OF CHARGE STATE DISTRIBUTIONS OF ''NEW'' CATHODE MATERIALS

Experiments and calculations show that there exist groups of similar elements. Many features behave periodically and this allows prediction of the CSDs of metals that have so far never been used as vacuum arc cathodes. By comparison with similar elements, effective freezing temperatures and densities have been determined for each ''new'' element under the conditions of low current and without magnetic fields [59]. Saha calculations have been performed in the same manner as described before (Sec. IV) and the resulting CSD are included in Table IV.

A legitimate question is how reliable these predictions are. The CSD of some elements (B, Na, K, Rb, Cs, Fr, Ra, and Ga) are dominated by a single charge state, almost independent of the freezing parameters; thus it can be assumed that precisely these CSDs will be found in future experiments. The situation is related to the inverse problem of ''uncertain'' determination of effective freezing parameters from experimentally known CSD (comment U in Table IV).

In the other cases, the CSDs depend on the effective freezing parameters and a relatively large error in the ion percentages is possible (factor 2 or even more). However, the calculations are qualitatively meaningful because they predict dominant ion charge states and approximate mean charge states. Moreover, the grouping of element properties also allows one to predict that future experimental CSDs of Tc, Ru, Rh, Re, and Os will be broadened comparably to the present calculated CSDs because all similar elements (Nb, Mo, Hf, Ta, and W) show substantial broadening.

ACKNOWLEDGMENTS

I would like to thank my friend and colleague Thomas Schülke for his help in the numerical solution of the Saha equations. I also would like to acknowledge stimulating discussions with Andreas Förster, Simone Anders, Ian Brown, Burkhard Jüttner, Efim Oks, and Georgi Yushkov. This work was supported by the U.S. Department of Energy, Division of Advanced Energy Projects, under Contract No. DE-AC03-76SF00098.

[1] *Vacuum Arcs—Theory and Applications*, edited by J. M. Lafferty (Wiley, New York, 1980).
[2] *Handbook of Vacuum Arc Science and Technology*, edited by R. L. Boxman, D. M. Sanders, and P. J. Martin (Noyes, Park Ridge, NJ, 1995).
[3] B. Jüttner, IEEE Trans. Plasma Sci. **PS-15**, 474 (1987).
[4] G. A. Mesyats and D. I. Proskurovsky, *Pulsed Electrical Discharge in Vacuum* (Springer-Verlag, Berlin, 1989).
[5] R. P. P. Smeets, IEEE Trans. Plasma Sci. **17**, 303 (1989).
[6] R. P. P. Smeets, IEEE Trans. Plasma Sci. **20**, 439 (1992).
[7] H. C. Miller, Contrib. Plasma Phys. **29**, 223 (1989).
[8] H. Ehrich *et al.*, IEEE Trans. Plasma Sci. **18**, 895 (1990).
[9] H.-M. Katsch, M. Mausbach, and K. G. Müller, J. Appl. Phys. **67**, 3625 (1990).
[10] H. Rosenthal *et al.*, J. Phys. D **28**, 353 (1995).
[11] A. M. Dorodnov, A. N. Kuznetsov, and V. A. Petrosov, Pis'ma Zh. Tekh. Fiz. **5**, 1001 (1979) [Sov. Tech. Phys. Lett. **5**, 418 (1979)].
[12] A. V. Bolotov *et al.*, Pis'ma Zh. Tekh. Fiz. **15**, 53 (1989) [Sov. Tech. Phys. Lett. **15**, 436 (1989)].
[13] V. M. Lunev, V. G. Padalka, and V. M. Khoroshikh, Zh. Tekh. Fiz. **47**, 1491 (1977) [Sov. Phys. Tech. Phys. **22**, 858 (1977)].
[14] W. D. Davis and H. C. Miller, J. Appl. Phys. **40**, 2212 (1969).
[15] A. A. Plyutto, V. N. Ryzhkov, and A. T. Kapin, Zh. Eksp.

Teor. Fiz. **47**, 494 (1964) [Sov. Phys. JETP **20**, 328 (1965)].
[16] I. G. Brown, B. Feinberg, and J. E. Galvin, J. Appl. Phys. **63**, 4889 (1988).
[17] I. G. Brown and X. Godechot, IEEE Trans. Plasma Sci. **PS-19**, 713 (1991).
[18] A. Anders *et al.*, IEEE Trans. Plasma Sci. **PS-21**, 305 (1993).
[19] E. Oks *et al.*, Appl. Phys. Lett. **67**, 200 (1995).
[20] F. J. Paoloni and I. G. Brown, Rev. Sci. Instrum. **66**, 3855 (1995).
[21] I. G. Brown, Rev. Sci. Instrum. **65**, 3061 (1994).
[22] A. Anders *et al.*, Rev. Sci. Instrum. **67**, 1202 (1996).
[23] J. E. Galvin, I. G. Brown, and R. A. MacGill, Rev. Sci. Instrum. **61**, 583 (1990).
[24] I. G. Brown *et al.*, Nucl. Instrum. Methods Phys. Res. Sect. B **43**, 455 (1989).
[25] E. M. Oks *et al.*, IEEE Trans. Plasma Sci. **24**, 1174 (1996).
[26] C. R. Negus and N. J. Peacock, J. Phys. D **12**, 91 (1979).
[27] R. Beier and H.-J. Kunze, Z. Phys. A **285**, 347 (1978).
[28] A. Anders, S. Anders, and E. Hantzsche, IEEE Trans. Plasma Sci. **17**, 653 (1989).
[29] R. B. Baksht, A. P. Kudinov, and E. A. Litvinov, Pis'ma Zh. Tekh. Fiz. **43**, 146 (1973) [Sov. Phys. Tech. Phys. **18**, 94 (1973)].
[30] S. Anders, Contrib. Plasma Phys. **26**, 416 (1986).
[31] S. Anders and A. Anders, J. Phys. D **21**, 213 (1988).
[32] S. Anders and A. Anders, Contrib. Plasma Phys. **29**, 537 (1989).
[33] A. Anders *et al.*, Plasma Sources Sci. Technol. **1**, 263 (1992).
[34] C. Wieckert, Contrib. Plasma Phys. **27**, 309 (1987).
[35] N. B. Volkov and A. Z. Nemirovsky, J. Phys. D **24**, 693 (1991).
[36] N. Radic and B. Santic, in *Proceedings of the International Symposium on Discharges and Electrical Insulation in Vacuum, Paris, 1988*, edited by J. M. Buzzi and A. Septier (Éditions de Physique, Paris, 1988), p. 217.
[37] I. A. Krinberg and M. P. Lukovnikova, J. Phys. D **28**, 711 (1995).
[38] A. Anders *et al.*, IEEE Trans. Plasma Sci. **20**, 466 (1992).
[39] B. Jüttner, J. Phys. D Appl. Phys. **28**, 516 (1995).
[40] V. F. Puchkarev and M. B. Bochkarev, J. Phys. D **27**, 1214 (1994).
[41] W. B. Nottingham, Phys. Rev. **59**, 907 (1941).
[42] T. H. Lee, J. Appl. Phys. **31**, 924 (1960).
[43] B. Jüttner, J. Phys. D **14**, 1265 (1981).
[44] A. Anders, *A Formulary for Plasma Physics* (Akademie-Verlag, Berlin, 1990).
[45] W. Ebeling, W.-D. Kremp, and D. Kraeft, *Theory of Bound States and Ionization Equilibrium in Plasmas and Solids* (Akademie-Verlag, Berlin, 1976).
[46] V. E. Fortov and I. T. Yakubov, *Physics of Nonideal Plasma* (Hemisphere, New York, 1990).
[47] W. Ebeling, Contrib. Plasma Phys. **29**, 165 (1989).
[48] W. Ebeling, A. Förster, and R. Radtke, *Physics of Nonideal Plasmas* (Teubner Verlagsgesellschaft, Stuttgart, 1992).
[49] W. Ebeling *et al.*, *Thermophysical Properties of Hot Dense Plasma* (Teubner Verlagsgesellschaft, Stuttgart, 1991).
[50] H.-W. Drawin and P. Felenbok, *Data for Plasmas in Local Thermodynamic Equilibrium* (Gauthier-Villars, Paris, 1965).
[51] C. E. Moore, *Atomic Energy Levels*, Natl. Bur. Stand. (U.S.) Circ. No. 467 (U.S. GPO, Washington, DC, 1949), Vols. I, II, III.
[52] S. Bashkin and J. O. Stoner, *Atomic Energy-Level and Grotrian Diagrams, vol. II, Sulfur I–Titanium XXII* (North-Holland, Amsterdam, 1978).
[53] C. E. Moore, *Selected Tables of Atomic Spectra, A: Atomic Energy Levels CI–CVI*, Natl. Stand. Ref. Data Ser., Natl. Bur. Stand. (U.S.), No. 3 (U.S. GPO, Washington, DC, 1970), Sec. 3.
[54] D. R. Lide and H. P. R. Frederikse, *Handbook of Physics and Chemistry* (CRC, Boca Raton, FL, 1995).
[55] T. A. Carlson *et al.*, At. Data **2**, 63 (1970).
[56] J. E. Daalder, J. Phys. D **8**, 1647 (1975).
[57] V. A. Ivanov, B. Jüttner, and H. Pursch, IEEE Trans. Plasma Sci. **13**, 334 (1985).
[58] A. Anders, S. Anders, and I. G. Brown, J. Appl. Phys. **75**, 4900 (1994).
[59] A. Anders and T. Schülke, in *Proceedings of the XVIIth International Symposium on Discharges and Electrical Insulation in Vacuum*, edited by S. Anders and A. Anders (Lawrence Berkeley National Laboratory, Berkeley, 1996).
[60] I. G. Brown and H. Shiraishi, IEEE Trans. Plasma Sci. **18**, 170 (1990).
[61] S. Anders *et al.*, IEEE Trans. Plasma Sci. **21**, 440 (1993).
[62] J. Kutzner, Zesz. Nauk. Politech. Poznan. **39**, 35 (1991).